



# Effect of amorphicity of HVOF sprayed Fe-based coatings on their corrosion performances and contacting osteoblast behavior



Deyan Li <sup>a,b</sup>, Xiuyong Chen <sup>b,\*</sup>, Xidong Hui <sup>c</sup>, Jinpeng Wang <sup>b</sup>, Peipeng Jin <sup>a,\*</sup>, Hua Li <sup>b,\*</sup>

<sup>a</sup> School of Mechanical Engineering, Qinghai University, Xining 810016, China

<sup>b</sup> Key Laboratory of Marine Materials and Related Technologies, Key Laboratory of Marine Materials and Protective Technologies of Zhejiang Province, Ningbo Institute of Materials Technology and Engineering, Chinese Academy of Sciences, Ningbo 315201, China

<sup>c</sup> State Key Laboratory for Advanced Metals and Materials, University of Science and Technology Beijing, Beijing 100083, China

## ARTICLE INFO

### Article history:

Received 28 July 2016

Revised 21 December 2016

Accepted in revised form 22 December 2016

Available online 23 December 2016

### Keywords:

Fe-based amorphous coatings

Nanocrystallization treatment

Mechanical properties

Corrosion resistance

Biocompatibility

## ABSTRACT

Fe<sub>53</sub>Cr<sub>19</sub>Zr<sub>7</sub>Mo<sub>2</sub>C<sub>18</sub>Si coatings with amorphous/nanocrystalline hybrid structures were fabricated by high velocity oxy-fuel spray. Enhanced amorphicity of the coatings, 55.85%, has been achieved by the spray quenching of the starting feedstock with an amorphicity of 36.82%. Further examination of the coating after post-spray crystallization annealing at 750 °C was also conducted. Microstructure, microhardness, wear/corrosion resistance and biocompatibility of the coatings were systematically studied. Results show that the nanocrystallization treatment brought about increased microhardness and enhanced anti-wear performances. However, electrochemical and *in vitro* cell culture testing suggest that the full crystalline structure does not favor the anti-corrosion and biological performances while presence of the amorphous structure enhances corrosion resistance of the coatings and promotes attachment and proliferation of osteoblast cells on their surfaces. The results shed some light on developing amorphous metallic coatings for potential biomedical applications.

© 2016 Elsevier B.V. All rights reserved.

## 1. Introduction

In the past decades, amorphous alloys have attracted intensive attention for potential biomedical applications as surgical tools or load-bearing implants, due to their excellent anti-corrosion/wear performances, high strength and processing capabilities [1–5]. A dichotomy has emerged in the types of bulk metallic glasses for biomedical applications. One is bioinert biomaterials such as Ti-based, Zr-based and Fe-based metallic glasses for permanent devices, and the other is bioresorbable implants like Mg-based alloys [6]. Among bioinert biomaterials, Fe-based amorphous alloys show the unique advantages of excellent mechanical properties and favorable corrosion resistance, as well as sufficient biocompatibility and cost efficiency [7]. Recent studies have reported that bulk Fe-based amorphous alloys show better corrosion resistance than 316L in simulated body fluids and might be suitable for biomedical applications [8–10]. Fe<sub>55</sub>Cr<sub>20</sub>Mo<sub>5</sub>P<sub>13</sub>C<sub>7</sub> bulk metallic glass had high corrosion resistance in simulated body fluids (Hank's solution and artificial saliva solution) and excellent biocompatibility, suggesting their promising potential as biomaterials [9]. Wang et al. investigated the corrosion resistance and biocompatibility of three kinds of Fe-based bulk metallic glass, and their results indicate that all the three

Fe-based bulk metallic glass samples show better corrosion resistance in simulated body fluids and no cytotoxicity to murine fibroblast cells was realized, therefore Fe-based amorphous alloys show promises for biomedical applications [10]. However, challenges pertaining to development of biomedical applications of these amorphous alloys persist yet, predominantly due to the difficulties encountered in production of bulk quantities [11,12]. New processing approaches are therefore essentially needed for making the amorphous materials in desired dimensions.

Surface technique might be a potential alternative for making coatings of the amorphous materials, since it is virtually known that surfaces of biomedical materials are presumably the key for their functional applications. Fe-based amorphous coatings have been developed to improve surface hardness, wear and corrosion resistance of boilers, gas turbines, hydraulic turbine blades, and so on [13]. Spark plasma sintering [14] and laser cladding [15] have been attempted to fabricate the amorphous coatings. Thermal spray approaches such as plasma spray [16,17], arc spray [18], electrospark deposition [19], kinetic spray [20,21], and high velocity oxy-fuel (HVOF) [22,23], were evidenced effective in long-term surface protection of conventional biomedical 316L by providing Fe-based coatings with amorphous/nanocrystalline structures. It has been realized that the presence of nanocrystalline regions in amorphous matrix may decrease the corrosion resistance in comparison with fully amorphous structure [24–26]. However, knowledge about anti-corrosion properties of the coatings

\* Corresponding authors.

E-mail addresses: [chenxiuyong@nimte.ac.cn](mailto:chenxiuyong@nimte.ac.cn) (X. Chen), [jinpeng@hotmail.com](mailto:jinpeng@hotmail.com) (P. Jin), [lihua@nimte.ac.cn](mailto:lihua@nimte.ac.cn) (H. Li).

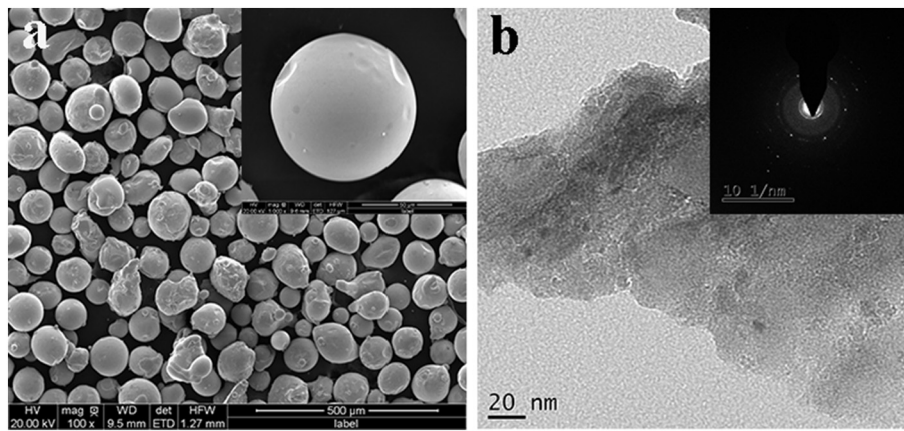


Fig. 1. FESEM (a) and TEM (b) images of the starting  $\text{Fe}_{53}\text{Cr}_{19}\text{Zr}_7\text{Mo}_2\text{C}_{18}\text{Si}$  powder.

in physiological media and their biocompatibility is insufficient. To date, however, there are few studies available on FeCrZrMoCSi amorphous alloys.

In this work,  $\text{Fe}_{53}\text{Cr}_{19}\text{Zr}_7\text{Mo}_2\text{C}_{18}\text{Si}$  coatings with amorphous/nano-crystalline hybrid structures were deposited onto 316L substrate by HVOF processing. Complete crystallization of the coatings was accomplished by additional annealing treatment. Effect of the annealing on microstructure, mechanical properties, corrosion resistance and biocompatibility of the coatings was assessed and elucidated. The results give clear insight into fabrication of Fe-based amorphous coatings for potential biomedical applications.

## 2. Materials and methods

$\text{Fe}_{53}\text{Cr}_{19}\text{Zr}_7\text{Mo}_2\text{C}_{18}\text{Si}$  powder with the size range of +30–150  $\mu\text{m}$  was used as the starting feedstock. Fabrication of the powder by high pressure argon gas atomization has been reported previously [27]. 316L stainless steel plates (316L) with the dimension of  $20 \times 20 \times 2$  mm were used as the substrates. The HVOF system (CJK5, Castolin Eutectic, Germany) was employed for making the coatings. Oxygen and kerosene were used as the combustion-supporting gas and fuel gas with the flow rate of 800 ml/min and 400 ml/min, respectively. Nitrogen was used as carrier gas with a flow rate of 8.5 ml/min. The powder feeding rate was 35 g/min and the spray distance was 30 cm. Thermal behavior of the as-sprayed coating was examined by differential scanning calorimetry (DSC, NETZSCH 404C, Germany) in a flow of nitrogen atmosphere at a heating rate of 20  $^{\circ}\text{C}/\text{min}$ . Based on the DSC analysis, further crystallization treatment was carried out by heating

the as-sprayed coatings at 750  $^{\circ}\text{C}$  for 1 h and naturally cooled to room temperature in a furnace.

Microstructure of the powder and coatings was characterized by field emission scanning electron microscopy (FESEM, FEI Quanta FEG250, the Netherlands) equipped with energy dispersive X-ray spectroscopy (EDS) and transmission electron microscopy (TEM, FEI Tecnai F20, the Netherlands). Phase composition of the samples was determined by X-ray diffraction (XRD, D8 Advance, Bruker AXS, Germany) using  $\text{Cu K}\alpha$  radiation operated at a scanning rate of  $0.1^{\circ}/\text{s}$  using  $\text{Cu K}\alpha$  radiation operated at 40 kV. The goniometer was set at a scan rate of  $0.033^{\circ}/\text{s}$  over a  $2\theta$  range of  $20^{\circ}$ – $90^{\circ}$ . Amorphicity of the powder and the as-sprayed coating was calculated from their XRD patterns. The XRD peaks were analyzed and fitted by Jade software, and amorphicity was calculated according to the equation:  $X_a = 1 - \frac{I_c}{I_c + I_a} \times 100\%$ , where  $X_a$  is amorphicity,  $I_a$  and  $I_c$  are amorphous scattering intensity and crystal diffraction intensity, respectively. Microhardness of the coatings was measured using a Vickers hardness tester (HV-1000, Shanghai Lianer Testing Equipment Co., China). A load of 100 g was applied and the microhardness value was reported based on the average of 10 measurements. Wear resistance of the coatings was evaluated by wet wear testing in phosphate buffered saline (PBS) using a ball-on-plate linear wear tester (MFT5000, Rtec Instruments, Inc., USA) with a load of 10 N and a sliding time of 30 min.  $\text{Al}_2\text{O}_3$  ball with a diameter of 6 mm was used as the counterpart material and new balls were used for each time testing. Wear volume loss was calculated from  $V = S \times d$ , where  $V$  referred to the wear volume ( $\text{mm}^3$ ),  $S$  was the cross sectional area ( $\text{mm}^2$ ) of the worn surfaces measured by a surface profile measuring instrument (Alpha-Step IQ, KLA-Tencor, USA),  $d$  was the oscillating

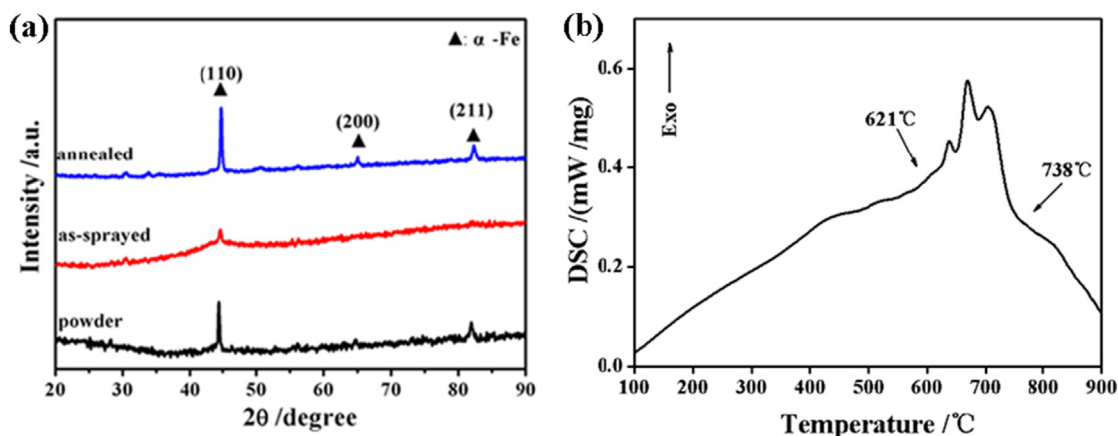
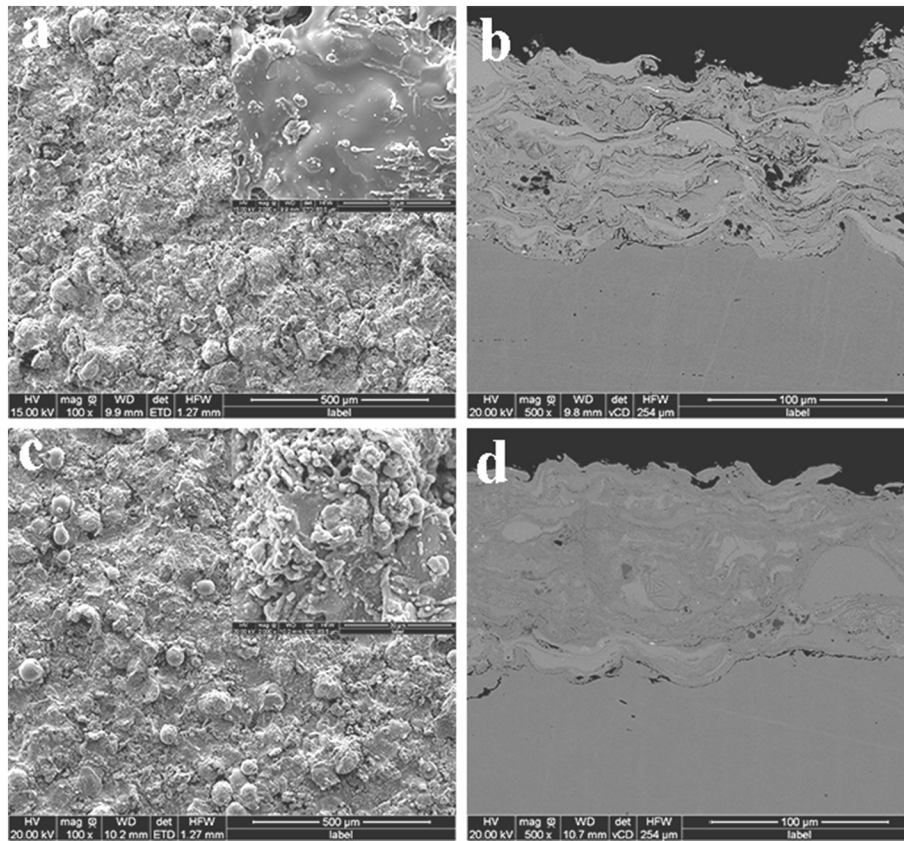


Fig. 2. (a) XRD patterns of the powder, the as-sprayed and the annealed coatings, and (b) DSC spectrum of the as-sprayed coating.



**Fig. 3.** FESEM images of the topographical and cross-sectional morphologies of the as-sprayed coatings (a, b) and the annealed coatings (c, d) (the insets are enlarged views of selected area in (a) and (c), respectively, scale bar: 30 μm).

stroke (mm). Five replicates were collected for the wear loss testing. Electrochemical behavior of the coatings was examined by potentiodynamic polarization testing in PBS (pH = 7.4) using a PGSTAT302 electrochemical workstation equipped with a three-electrode cell system. Platinum electrode was used as the counter electrode, the sample was used as the working electrode, and a saturated calomel electrode was used as the reference electrode. Polarization curves were recorded with a potential sweep rate of 0.5 mV/s after immersing the samples for one hour. The samples for the electrochemical measurements were polished to mirror finish in order to obtain identical surface roughness, followed by ultrasonic cleaning with acetone, alcohol and distilled water in turn and finally dried with warm air. After polarization, concentration of the ions released from the samples into the electrolytes

was determined by an inductively coupled plasma optical emission spectrometer (ICP-OES, PE Optima 2100DV, Perkin-Elmer, USA) and the surfaces of the samples were characterized by FESEM.

Cell culturing was carried out for the coating samples using human osteoblasts (HFOB 1.19 SV40 transfected osteoblasts). 316 L plates were used as the control samples. Cell viability was evaluated by MTT assay. Briefly, cells were cultured for 1 day, 3 days, and 5 days, respectively. Then, 20 μl of MTT (5 mg/ml, Sigma, St Louis, MO, USA) was added to each well and incubated at 37 °C for another 4 h. MTT-containing media was removed and 100 μl dimethyl sulfoxide (DMSO) was added to dissolve the formed formazan crystals. Optical density of the solution was measured at a wavelength of 490 nm using a microplate reader (SpectraMax 190, MD, USA). Morphology of the attached

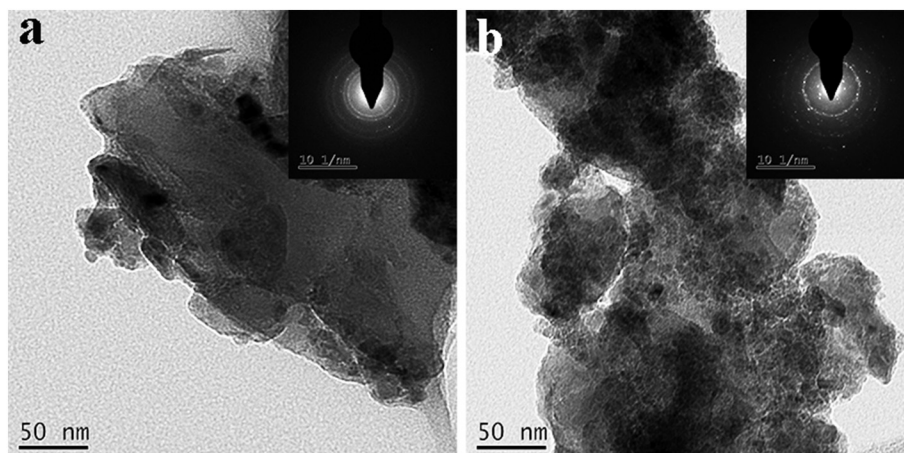


**Fig. 4.** TEM images of the as-sprayed coating (a) and the annealed coating (b).

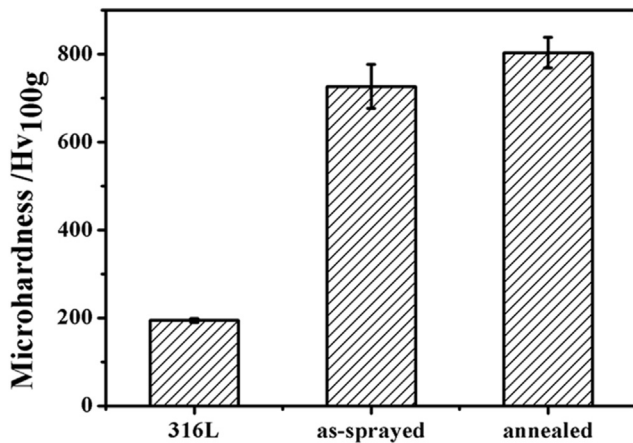


Fig. 5. Vickers hardness of the 316L, the as-sprayed coating and the annealed coating.

osteoblasts on different samples was observed with FESEM. For the culturing, cells were seeded at an initial density of  $1 \times 10^4$  cells/ml. After cultured for 1, 3 and 5 days, cells were washed with phosphate-buffered saline (PBS, pH = 7.4) and fixed with 2.5% glutaraldehyde for 24 h. The samples were finally dehydrated for FESEM observation. All data were expressed as means  $\pm$  standard deviations (SD) of 3 replicates. The statistical analysis was performed using Student's *t*-test and one-way analysis of variance (ANOVA) at confidence levels of 95 and 99% (OriginPro version 7.5).

### 3. Results and discussion

#### 3.1. Structure of powder and coatings

SEM characterization of the gas-atomized powder shows near-spherical contour of the particles with the size of  $\sim 30$ – $150 \mu\text{m}$  in diameter (Fig. 1a). The relative smooth surface ensures favorable fluidity for thermal spray processing. TEM image and the corresponding selected area electron diffraction (SAED) pattern (the inset in Fig. 1b) further reveal the amorphous structure in the powder (Fig. 1b). Nanocrystalline phases are also suggested in the starting particles. The diffused halo ring in the SAED pattern reveals that the powder has an amorphous structure. Meanwhile, the diffraction spots indicate the existence of crystals in the powder. This result agrees well with the XRD results (Fig. 2a).

Chemical composition of the as-sprayed coating is  $\text{Fe}_{53}\text{Cr}_{19}\text{Zr}_7\text{Mo}_2\text{C}_{18}\text{Si}$  (at.%) as obtained by EDS analysis. The annealing

temperature,  $750^\circ\text{C}$ , was selected based on the DSC analysis (Fig. 2b). It is clear that the as-sprayed coatings show a multi-step crystallization process. The large exothermic peak is associated with the crystallization of the existing amorphous structure. It is noted that amorphicity of the starting feedstock powder is 36.82% with certain amount of nanocrystalline. This is similar to a previous study reported for similar Fe-based amorphous powder [28]. Interestingly, after the HVOF deposition, the crystalline peaks in the as-sprayed coating are notably weaker than those in the powder, showing enhanced amorphicity to 55.85% (Fig. 2a). This phenomenon is likely owing to a high cooling rate attained by the particles in molten state during flattening-solidification stage as compared with the gas-atomizing processing [2]. It is not surprising to obtain the entire crystallization of the phases in the annealed coatings (Fig. 2a). The XRD curve for the as-sprayed coatings shows a broad halo peak at the  $2\theta$  angles of  $40^\circ$ – $50^\circ$ , suggesting promoted amorphicity of the coating as compared to the starting powder. A small amount of crystalline diffraction peaks are also discerned. The as-sprayed coatings are partially amorphous with presence of limited amount of crystalline phases. The major crystalline phase with cubic structure and a lattice parameter of 0.2866 nm is assigned to  $\alpha$ -Fe (JCPDS Card No.: 65-4899), and it is uniformly embedded in the amorphous matrix. The special hybrid structure comprising both amorphous and nanocrystalline phases would play crucial roles in affecting their performances.

Further SEM observation discloses the structural evolution of the amorphous phase into crystalline structures (Fig. 3). It is clear that surface morphology of the as-sprayed coating with the thickness of  $\sim 150 \mu\text{m}$  shows well-flattened splats, while simultaneously exhibits some heterogeneous phases, such as unmolten particles and intersplat regions (Fig. 3a). In addition, micron-sized pores are seen from the cross-sections of the as-sprayed coating, while dense layer structure is revealed (Fig. 3b). After the heat treatment, densified structure with diminished flaws is seen (Fig. 3c, d). Weakened splats' interfaces indicate presumable occurrence of diffusion and sintering during the post-spray heat treatment (Fig. 3d). To further elucidate the structures, TEM characterization was performed (Fig. 4). It is further suggested that majority of the phases in the as-sprayed coating are amorphous in nature. Nevertheless, nanocrystalline grains can be ascertained from the diffused halo ring in the SAED pattern. It should be noted that content of the amorphous phase in the as-sprayed coating already exceeds that in the initial powder. Compared to the as-sprayed coating, much more nanocrystalline grains are formed in the annealed coating. This phenomenon is consistent with the XRD results of the coatings (Fig. 2a). The grains existing in the annealed coating show the size of  $< 6 \text{ nm}$  (Fig. 4b). It is likely that the nanocrystalline grains originate predominantly from the initial nano grains and crystallization of the amorphous matrix further facilitates their formation.

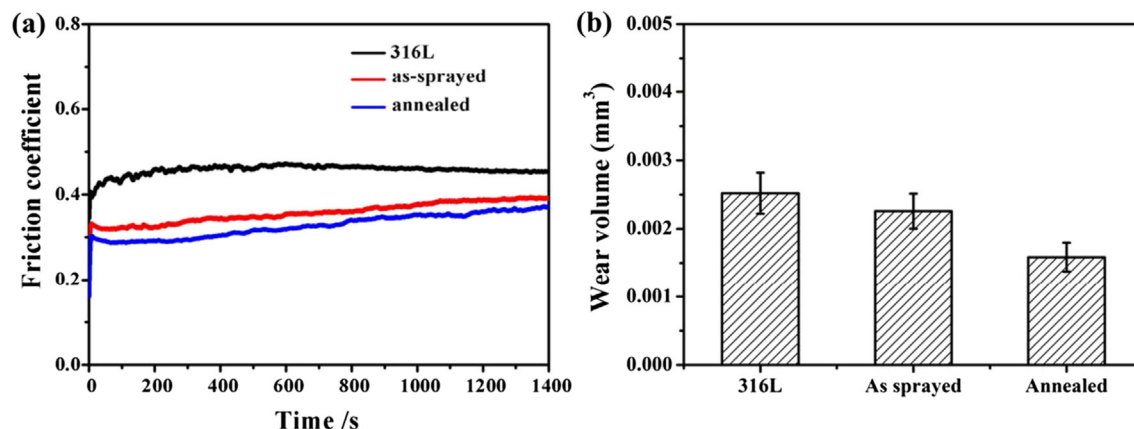


Fig. 6. Friction coefficient (a) and volume loss (b) of the 316L, the as-sprayed and the annealed coatings acquired during the wet sliding wear testing in PBS.

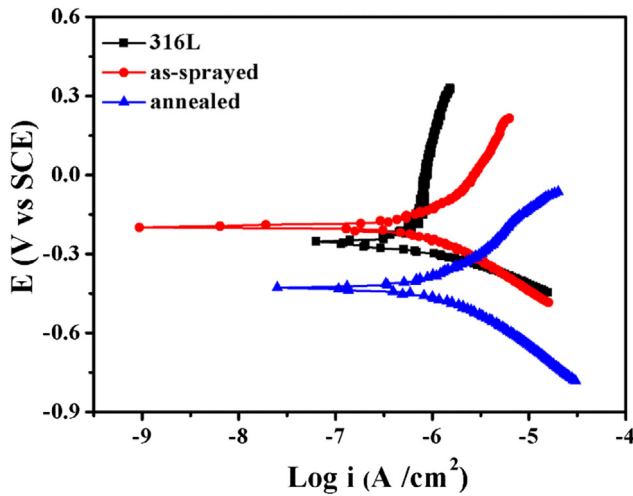


Fig. 7. Potentiodynamic polarization curves of the 316L, the as-sprayed and the annealed coatings tested in PBS.

### 3.2. Mechanical properties of the coatings

It is noted that the crystallization treatment results in slight increase in microhardness, from  $726.78 \pm 49.58$  Hv to  $803.59 \pm 37.77$  Hv (Fig. 5). The microhardness values of the as-sprayed and the annealed coatings are much higher than that of 316L plates, giving rise to significantly improved wear resistance. The relatively higher microhardness value of the annealed coatings could be triggered by the denser structure. Moreover, the precipitates of Mo and Cr, which are usually formed in sintering-induced lamella structure, can enhance the microhardness of amorphous alloys [29].

Wet sliding testing of the coatings in PBS environment shows that both the as-sprayed and the completely crystallized coatings have lower COF values than that of 316L plates (Fig. 6). However, the as-sprayed coating exhibits higher steady state COF value of 0.370, slightly higher than that of the annealed coating, 0.342. Wear loss of the 316L substrate and the as-sprayed coating are slightly higher than that of the annealed coating, while the slight differences indicate favorable wear resistance of the annealed coating. This agrees well with the microhardness results. The nanocrystallization of the amorphous phase presumably accounts mainly for the high wear resistance, since fine grain strengthening through blocking dislocation movement plays crucial roles during sliding wear [30]. Nevertheless, both the as-sprayed and the annealed Fe-based coatings are promising for protecting 316L substrates by withstanding frictional wear.

### 3.3. Corrosion and biocompatibility of the coatings

The purpose of adding Cr, Zr Mo and Si to the Fe-based alloy was predominately to improve its corrosion resistance. It is known that Cr is an

important element to increase the corrosion resistance through forming stable and dense chromium oxide passive film. The addition of Mo in the amorphous alloys can promote the enrichment of Cr in the passive film, thus further improving the corrosion resistance. Si element also helps to promote the corrosion resistance of the amorphous coatings through the formation of  $\text{SiO}_2$  passive film. Furthermore, Zr favors biocompatibility of the alloy, which is very important for its potential biomedical applications. In addition, toxic and potentially harmful elements, such as Ni, are avoided. Interestingly, it is noted that the crystallization treatment triggers deteriorated corrosion resistance of the coatings (Fig. 7). Corrosion potential ( $E_{\text{corr}}$ ) and corrosion current densities ( $I_{\text{corr}}$ ) of the samples were estimated from their polarization curves. Apparently, with smaller  $I_{\text{corr}}$  value and higher  $E_{\text{corr}}$  value acquired in PBS, the as-sprayed coatings are more corrosion-resistant than 316L. The as-sprayed coatings exhibit the hybrid structure comprising both amorphous and nanocrystalline phases with  $\alpha$ -Fe, Cr-rich or Mo-rich nanosize phases being uniformly embedded in amorphous matrix. It is possible that the ultrafine nanocrystalline phases result in uniform distribution of impurities and provide homogenous substrate for the formation of a passive layer, consequently improving the corrosion resistance [9,31]. In addition, the higher corrosion resistance of the as-sprayed coatings can be attributed to their chemical homogeneity and less structural defects [10]. However, the annealed coating shows higher  $I_{\text{corr}}$  and lower  $E_{\text{corr}}$  than those of the as-sprayed coatings, implying decreased corrosion resistance of the coatings after the crystallization treatment. Complete crystallization treatment usually leads to formation of grain boundaries, crystalline defects or segregates, which usually act as the corrosion initiation sites [24]. In fact, obvious pitting is realized on the 316L plate after the polarization in PBS solution (Fig. 8a). While barely any pits could be observed for the as-sprayed coating (Fig. 8b), indicating good corrosion resistance of the as-sprayed coating. Moreover, the pits on the annealed coating are more remarkable and larger in size than those on 316L (Fig. 8c versus a), indicating more severe corrosion demonstrated by the crystallized coating. This result is consistent with the electrochemical testing data (Fig. 7). It is therefore clear that corrosion resistance of the amorphous coating is deteriorated after the post-spray heat treatment. Generation of abundant grain boundaries should account for the easy appearance of pitting, since pits are always initiated at the boundaries. In addition, passive films formed on the as-sprayed amorphous coating could explain the less pitting of the coating immersed in the PBS solution. Similar result was reported that less amount of passivating alloying elements, such as Cr, are required to form more uniform and stable passive film on Fe-based amorphous alloys [31]. Chemical heterogeneities do not occur in the amorphous structure and a chemically homogeneous single phase is attained owing to a high cooling rate.

For biomedical applications, constrained release of metal ions from the coatings is essential for their long-term functional services. The metal ions released from the samples after the polarization in PBS were measured using ICP-OES. It is noted that no metal ions are detected in the solution for the 316L plates after the corrosion testing. The

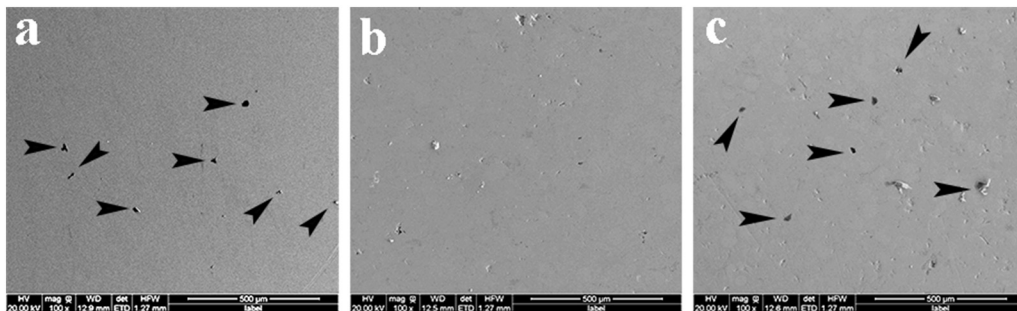


Fig. 8. FESEM micrographs of (a) the 316L, (b) the as-sprayed coating, and (c) the annealed coating, showing clear pitting on the 316L plate and the annealed coating after the polarization testing in PBS.

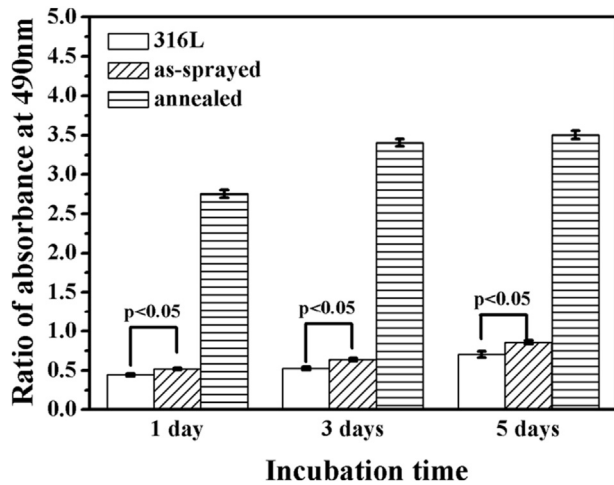


Fig. 9. Cell viability of human osteoblasts cultured on the surfaces of the 316L, the as-sprayed and the annealed coatings. Error bars represent mean  $\pm$  SD for  $n = 3$ .

concentration of metal ions released from the as-sprayed coatings is also below the detection limit, which is consistent with their high corrosion resistance. However, for the annealed coatings, significant amount of Fe and Cr ions are detected at the level of 787  $\mu\text{g/l}$  and 34  $\mu\text{g/l}$ , respectively. It was reported that high concentration of Fe and Cr ions probably restrains the viability of human osteoblast and causes the toxicity to human body [32–34]. In this case, MTT assay was employed to evaluate the cytotoxicity of all the samples. Fig. 9 shows the absorbance data of

formazan produced by the osteoblasts adhered on the different samples. After culturing for 1 day, the osteoblasts adhered on the as-sprayed coatings display significantly higher ( $p < 0.05$ ) cell viability than those adhered on 316L plates. However, the osteoblasts adhering on the annealed coatings show significantly higher cell viability than those on the 316L substrate. After culturing for 3 and 5 days, similar result was observed for the samples. This abnormal phenomenon occurred for the annealed coatings might be related to the fact that the Fe and Cr ions released from the coatings likely adhere on the surface of cells or the inwall of the culturing well, this in turn results in enhanced absorbance. This phenomenon has been validated that the value of absorbance in MTT assay is greatly influenced by the color of tested materials [35]. To further examine the cytotoxicity of the samples, SEM images of the human osteoblasts attached on the different samples after different culturing durations were acquired, as shown in Fig. 10. It is noted that the cells show flattened and well spreading morphology on the surfaces of the 316L plate (Fig. 10a) and the as-sprayed coating (Fig. 10b). Additionally, there are few cells attaching on the surface of the annealed coating after 1 day incubation and no cell was observed after 3 days incubation. Instead, a large quantity of harmful corrosion products ascribed to Cr-related or Fe-related compounds on the surface of the annealed coating are seen after 3 days culturing, which are confirmed by EDS analysis (Fig. 10d). Taking into account the high corrosion resistance and less cytotoxicity of the coating, the as-sprayed Fe-based coating with amorphous/nanocrystalline hybrid structures shows great promise as biomedical layer. It was reported that Cr ions could induce cytotoxicity and oxidative stress [36] and reduced the osteoprotegerin (OPG)/receptor activator of nuclear factor kappa B ligand (RANKL) ratio on MG-63 human osteoblast-like cells [37] when their

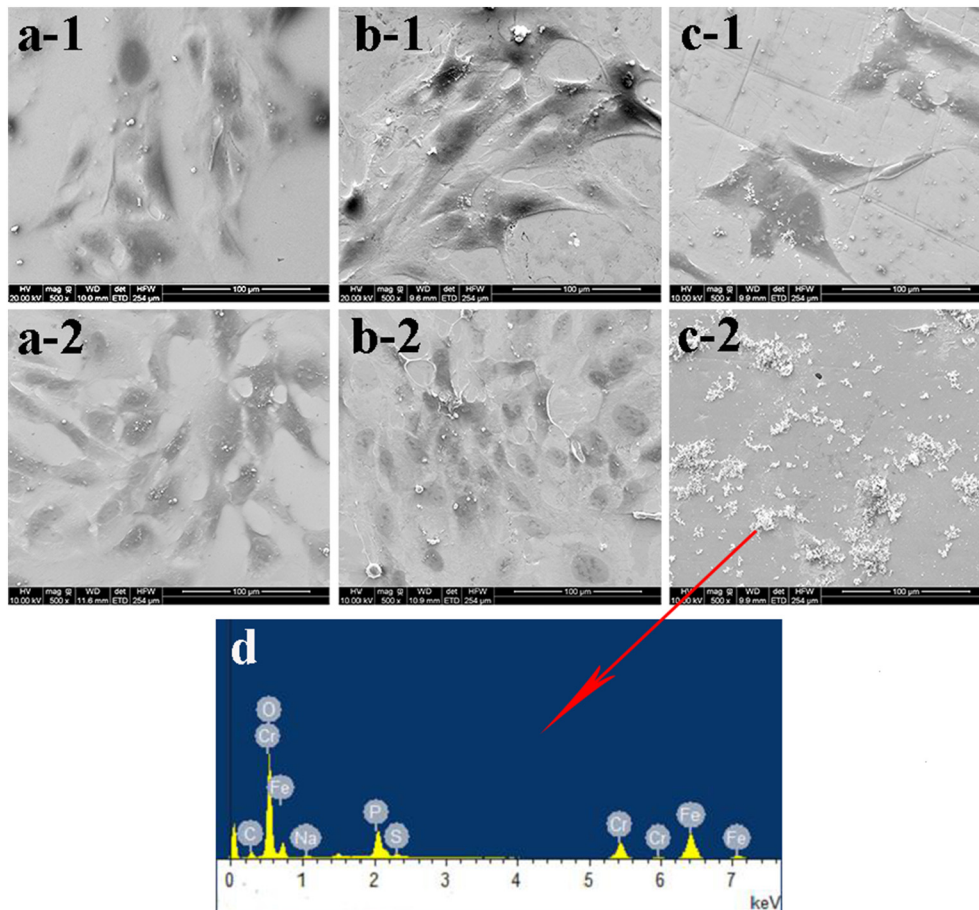


Fig. 10. FESEM micrographs of human osteoblasts cultured on the surfaces of (a) the 316 L plate, (b) the as-sprayed coating, and (c) the annealed coating for 1 day (–1) and 3 days (–2), and (d) EDS analysis of the corrosion products formed on the surface of the annealed coatings after 3 days of incubation.

concentration reached certain values. Our results indicate that Cr ions in low level might offer the potential to modify the redox state of the human cells and protein function. Yet, regardless of the encouraging performances of the Fe-based amorphous coating, a variety of testing is still needed to examine their mechanical and biological properties for potential biomedical applications. Nevertheless, coating fabrication by HVOF of amorphous alloys might open a new window for processing amorphous biomedical alloys.

#### 4. Conclusions

Fe<sub>53</sub>Cr<sub>19</sub>Zr<sub>7</sub>Mo<sub>2</sub>C<sub>18</sub>Si coatings with 55.85% amorphicity have been successfully fabricated by high velocity oxy-fuel spray. Crystallographic coatings were obtained by post-spray heat treatment at 750 °C. The completely crystallized coatings show enhanced anti-wear performances, while the heat treatment deteriorates corrosion resistance of the coatings in simulated body fluid. Presence of the amorphous phase gives rise to promoted corrosion resistance in simulated body fluid and favor attachment and proliferation of osteoblast cells. The amorphous/nanocrystalline coatings show good mechanical properties, high corrosion resistance in physiological media and excellent biocompatibility, making it a promising material for biomedical applications. The results give certain insight into processing amorphous alloys for potential biomedical applications.

#### Acknowledgements

This work was supported by the National Natural Science Foundation of China (grant # 51401232, 41476064 and 31271017).

#### References

- [1] W.J. Botta, J.E. Berger, C.S. Kiminami, V. Roche, R.P. Nogueira, C. Bolfarini, Corrosion resistance of Fe-based amorphous alloys, *J. Alloys Compd.* 586 (2014) S105–S110.
- [2] R.Q. Guo, C. Zhang, Q. Chen, Y. Yang, N. Li, L. Liu, Study of structure and corrosion resistance of Fe-based amorphous coatings prepared by HVOF and HVOF, *Corros. Sci.* 53 (2011) 2351–2356.
- [3] C.H. Lin, C.H. Huang, J.F. Chuang, H.C. Lee, M.C. Liu, X.H. Du, J.C. Huang, J.S.C. Jang, C.H. Chen, Simulated body-fluid tests and electrochemical investigations on biocompatibility of metallic glasses, *Mater. Sci. Eng. C* 32 (2012) 2578–2582.
- [4] W. Wang, C. Zhang, P. Xu, M. Yasir, L. Liu, Enhancement of oxidation and wear resistance of Fe-based amorphous coatings by surface modification of feedstock powders, *Mater. Des.* 73 (2015) 35–41.
- [5] K. Hashimoto, What we have learned from studies on chemical properties of amorphous alloys? *Appl. Surf. Sci.* 257 (2011) 8141–8150.
- [6] P. Meagher, E.D. O'Carbhaill, J.H. Byrne, D.J. Browne, Bulk metallic glasses for implantable medical devices and surgical tools, *Adv. Mater.* 28 (2016) 5755–5762.
- [7] Y.M. Sun, Y.G. Wang, J.T. Zhang, R. Li, L.Y. Guo, H. Xu, W.M. Wang, Effect of casting vacuum on thermodynamic and corrosion properties of Fe-based glassy alloy, *T. Nonferr. Metal. Soc.* 25 (2015) 844–849.
- [8] J. Schroers, G. Kumar, T.M. Hodges, S. Chan, T.R. Kyriakides, Bulk metallic glasses for biomedical applications, *JOM* 61 (2009) 21–29.
- [9] S. Li, Q. Wei, Q. Li, B. Jiang, Y. Chen, Y. Sun, Development of Fe-based bulk metallic glasses as potential biomaterials, *Mater. Sci. Eng. C* 52 (2015) 235–241.
- [10] Y.B. Wang, H.F. Li, Y.F. Zheng, M. Li, Corrosion performances in simulated body fluids and cytotoxicity evaluation of Fe-based bulk metallic glasses, *Mater. Sci. Eng. C* 32 (2012) 599–606.
- [11] C. Su, Y. Chen, P. Yu, M. Song, W. Chen, S.F. Guo, Linking the thermal characteristics and mechanical properties of Fe-based bulk metallic glasses, *J. Alloys Compd.* 663 (2016) 867–871.
- [12] C.L. Zhu, Q. Wang, F.W. Li, Y.H. Li, Y.M. Wang, C. Dong, W. Zhang, A. Inoue, Cluster-based bulk metallic glass formation in Fe-Si-B-Nb alloy systems, *J. Phys. Conf. Ser.* 144 (2009) 012048.
- [13] J.B. Cheng, X.B. Liang, Y.X. Chen, Z.H. Wang, B.S. Xu, High-temperature erosion resistance of FeSiNb amorphous coatings deposited by arc spraying for boiler applications, *J. Therm. Spray Technol.* 22 (2012) 820–827.
- [14] A. Singh, S.R. Bakshi, A. Agarwal, S.P. Harimkar, Microstructure and tribological behavior of spark plasma sintered iron-based amorphous coatings, *Mater. Sci. Eng. A* 527 (2010) 5000–5007.
- [15] Q. Zhou, S. Qu, X. Wang, Z. Zou, Synthesis of Fe-based amorphous composite coatings with low purity materials by laser cladding, *Appl. Surf. Sci.* 253 (2007) 7060–7064.
- [16] K. Kishitake, H. Era, F. Otsubo, Characterization of plasma sprayed Fe-17Cr-38Mo-4C amorphous coatings crystallizing at extremely high temperature, *J. Therm. Spray Technol.* 5 (1996) 283–288.
- [17] F. Otsubo, K. Kishitake, Corrosion resistance of Fe-16%Cr-30%Mo-(C,B,P) amorphous coatings sprayed by HVOF and APS processes, *Mater. Trans.* 46 (2005) 80–83.
- [18] J. Cheng, D. Liu, X. Liang, Y. Chen, Wear behaviors of arc-sprayed FeSiNb amorphous coatings, *Tribol. Lett.* 60 (2015) 1–7.
- [19] S. Cadney, M. Brochu, Formation of amorphous Zr<sub>41.7</sub>Ti<sub>13.8</sub>Ni<sub>10</sub>Cu<sub>12.5</sub>Be<sub>22.5</sub> coatings via the ElectroSpark deposition process, *Intermetallics* 16 (2008) 518–523.
- [20] A.P. Wang, T. Zhang, J.Q. Wang, Ni-based fully amorphous metallic coating with high corrosion resistance, *Philos. Mag. Lett.* 86 (2006) 5–11.
- [21] S. Yoon, H.J. Kim, C. Lee, Deposition behavior of bulk amorphous NiTiZrSiSn according to the kinetic and thermal energy levels in the kinetic spraying process, *Surf. Coat. Technol.* 200 (2006) 6022–6029.
- [22] M. Cherigui, N.E. Fenineche, C. Coddet, Structural study of iron-based microstructured and nanostructured powders sprayed by HVOF thermal spraying, *Surf. Coat. Technol.* 192 (2005) 19–26.
- [23] Y. Wu, P. Lin, G. Xie, J. Hu, M. Cao, Formation of amorphous and nanocrystalline phases in high velocity oxy-fuel thermally sprayed Fe-Cr-Si-B-Mn alloy, *Mater. Sci. Eng. A* 430 (2006) 34–39.
- [24] Y. Yang, C. Zhang, Y. Peng, Y. Yu, L. Liu, Effects of crystallization on the corrosion resistance of Fe-based amorphous coatings, *Corros. Sci.* 59 (2012) 10–19.
- [25] M.J. Duarte, A. Kostka, J.A. Jimenez, P. Choi, J. Klemm, D. Crespo, D. Raabe, F.U. Renner, Crystallization, phase evolution and corrosion of Fe-based metallic glasses: an atomic-scale structural and chemical characterization study, *Acta Mater.* 71 (2014) 20–30.
- [26] H.M. Ha, J.H. Payer, Devitrification of Fe-based amorphous metal SAM 1651: a structural and compositional study, *Metall. Mater. Trans. A* 40 (2009) 2519–2529.
- [27] Y.F. Zhao, J.J. Si, J.G. Song, X.D. Hui, High strength Mg-Zn-Ca alloys prepared by atomization and hot pressing process, *Mater. Lett.* 118 (2014) 55–58.
- [28] K. Chokethawai, D.G. McCartney, P.H. Shipway, Microstructure evolution and thermal stability of an Fe-based amorphous alloy powder and thermally sprayed coatings, *J. Alloys Compd.* 480 (2009) 351–359.
- [29] B.Y. Fu, D.Y. He, L.D. Zhao, Effect of heat treatment on the microstructure and mechanical properties of Fe-based amorphous coatings, *J. Alloys Compd.* 480 (2009) 422–427.
- [30] Z. Zhou, L. Wang, D.Y. He, F.C. Wang, Y.B. Liu, Y.B. Liu, Microstructure and wear resistance of Fe-based amorphous metallic coatings prepared by HVOF thermal spraying, *J. Therm. Spray Technol.* 19 (2010) 1287–1293.
- [31] C.A.C. Souza, D.V. Ribeiro, C.S. Kiminami, Corrosion resistance of Fe-Cr-based amorphous alloys: an overview, *J. Non Cryst. Solids* 442 (2016) 56–66.
- [32] S.J. Soenen, U. Himmelreich, N. Nuytten, M. De Cuyper, Cytotoxic effects of iron oxide nanoparticles and implications for safety in cell labelling, *Biomaterials* 32 (2011) 195–205.
- [33] A.J. Ortiz, E. Fernandez, A. Vicente, J.L. Calvo, C. Ortiz, Metallic ions released from stainless steel, nickel-free, and titanium orthodontic alloys: toxicity and DNA damage, *Am. J. Orthod. Dentofac. Orthop.* 140 (2011) e115–e122.
- [34] A. Petit, F. Mwale, C. Tkaczyk, J. Antoniou, D.J. Zukor, O.L. Huk, Cobalt and chromium ions induce nitration of proteins in human U937 macrophages *in vitro*, *J. Biomed. Mater. Res. A* 79 (2006) 599–605.
- [35] P.W. Sylvester, Optimization of the tetrazolium dye (MTT) colorimetric assay for cellular growth and viability, *Methods Mol. Biol.* 716 (2011) 157–168.
- [36] C. Fleury, A. Petit, F. Mwale, J. Antoniou, D.J. Zukor, M. Tabrizian, O.L. Huk, Effect of cobalt and chromium ions on human MG-63 osteoblasts *in vitro*: morphology, cytotoxicity, and oxidative stress, *Biomaterials* 27 (2006) 3351–3360.
- [37] W.P. Zijlstra, S.K. Bulstra, J.J.A.M. van Raay, B.M. van Leeuwen, R. Kuijjer, Cobalt and chromium ions reduce human osteoblast-like cell activity *in vitro*, reduce the OPG to RANKL ratio, and induce oxidative stress, *J. Orthop. Res.* 30 (2012) 740–747.